Excited-State AIE Material for Differential Recognition of Toxic Hair Color Ingredients: Towards Functional Device Applications

Shagun,[a] Deekshit Dhiman,[b] Darsi Rambabu,[c] Koen Robeyns,[c] Robin Khosla[b] and Abhimanew Dhir*[a]

[a] *School of Chemical Sciences, Indian Institute of Technology Mandi, Kamand, Himachal Pradesh-175005, India*
[b] *School of Computing and Electrical Engineering, Indian Institute of Technology Mandi, Kamand, Himachal Pradesh-175005, India*
[c] *Institute of Condensed Matter and Nanosciences, Molecular Chemistry, Materials and Catalysis, Université catholique de Louvain, Louvain-la-Neuve B-1348, Belgium*

Corresponding author email: abhimanew@iitmandi.ac.in

(Supplementary Information)

Contents

General Information

1. Materials and Instrumentation: All commercially available chemicals and analytical grade solvents were purchased from reliable sellers and used without further purification. The hair color utilized for commercial hair color study was purchased from a local market. ^{1}H and ^{13}C NMR measurements were performed on a JEOL ECX 500 MHz spectrometer with TMS as internal standard. Mass-spectrometry was done using a HRMS Bruker Impact HD. Single crystal X-ray data were collected on a monochromated (multilayer optics) dual source (Cu and Mo) Bruker D8 Venture, equipped with an Eos CCD detector, using MoKα (λ = 0.71073) at 171K. Data acquisition, reduction and multi-scan absorption correction were performed with the Bruker apex4 suite. The structure was solved by SHELXT and refined by SHELXL2019/3. Ultraviolet-Visible absorbance spectra were recorded on UV-Visible spectrophotometer (Shimadzu UV-2450), fluorescence studies were performed using Agilent Fluorescence spectrometer (Cary eclipse)**.** Fluorescence lifetime measurements were done using a Delta Flex TCSPC system, Horiba Scientific with Pulsed LED sources. DLS was done on a Malvern Instruments Ltd Zetasizer Nano ZS. Scanning electron microscopy (FE-SEM, ZEISS, Gemini SEM 500) and Transmission electron microscopy (HR-TEM, Thermo Fisher, Tacnai G2 20 S-TWIN) facilities were used for microscopic imaging. For the fabrication of sensor devices, the Ti/Pt micro-Interdigitated Electrodes (IDE) are fabricated using DC magnetron sputtering on cleaned (acetone, IPA and DI ultrasonicated) glass substrate followed by deposition of sensor thin film using spin coating at 3000 rpm for 30sec. The current-voltage (I-V) characteristics were measured using Keithley SCS 4200 system.

2. Quantum yield: The quantum yield was calculated using the following equation:

$$\boldsymbol{Q_S = Q_R \frac{I_S A_R \eta_S^2}{I_R A_S \eta_R^2}}$$

where, Q_S = Quantum yield of sample, Q_R = Quantum yield of reference, I_S and I_R = Integrated Intensities of sample and reference respectively i.e. area under their emission spectra, A_R and A_S = Absorbance of reference and sample respectively, η_S and η_R = Refractive indices of sample and reference solvents.

3. Stern-Volmer plots: The Stern-Volmer quenching constant (K_{SV}) was calculated from the following equation:

$$\boldsymbol{\frac{I_0}{I} = 1 + Ksv[Q]}$$

The slope of the calibration plot [Q] (quencher concentration in M) vs I_0/I (ratio of Initial fluorescence intensity of the probe to the final intensity after the addition of quencher analyte) in the linear range, gives Stern-Volmer quenching constant (K_{SV}).

4. Limit of detection (LOD): The limit of detection (LOD) was determined by using the equation:

$$\mathbf{LOD = 3\delta/K}$$

where, δ = standard deviation of ten blank measurements, and K = slope of the calibration plot of analyte concentration vs I_0/I (ratio of Initial fluorescence intensity of the probe to the final intensity after the addition of analyte).

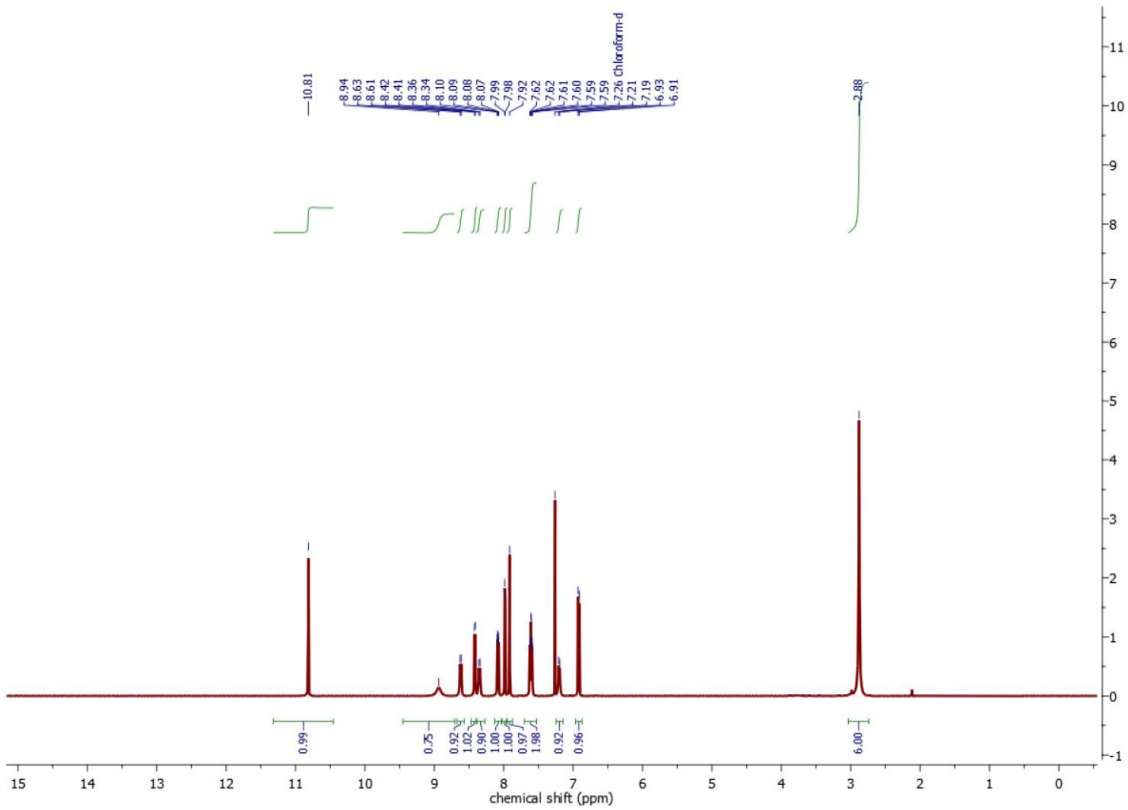

Figure S1. ^{1}H NMR spectrum of compound **DHNB** in $CDCl_3$.

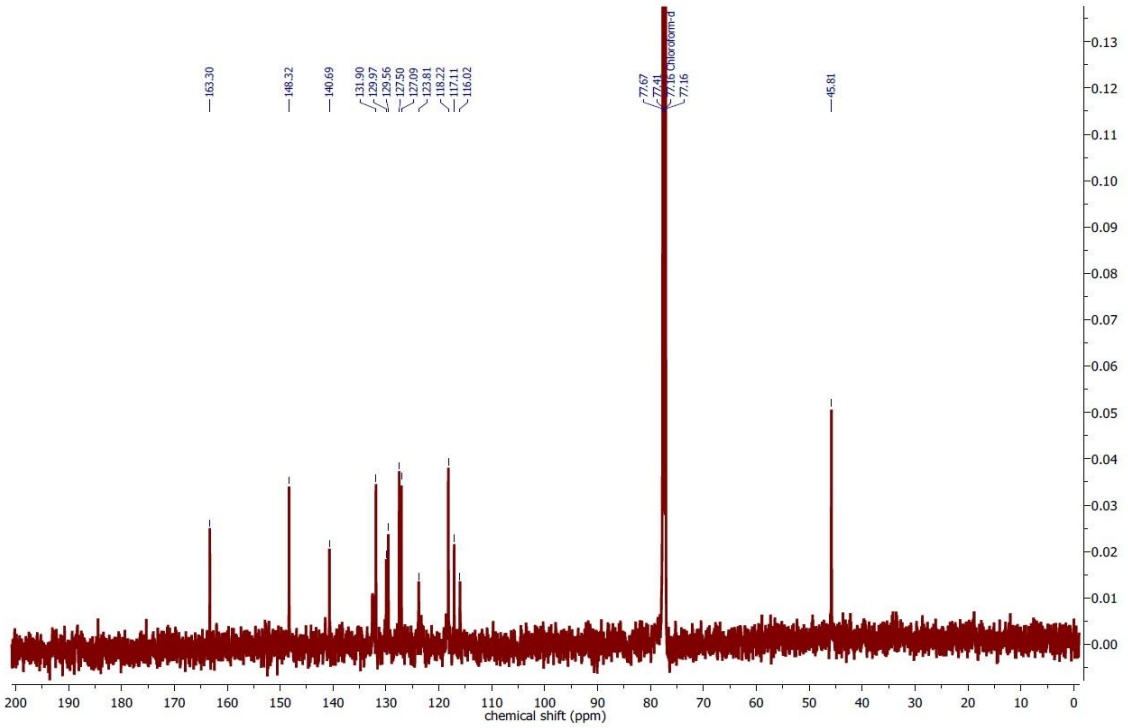

Figure S2. ^{13}C NMR spectrum of compound **DHNB** in $CDCl_3$.

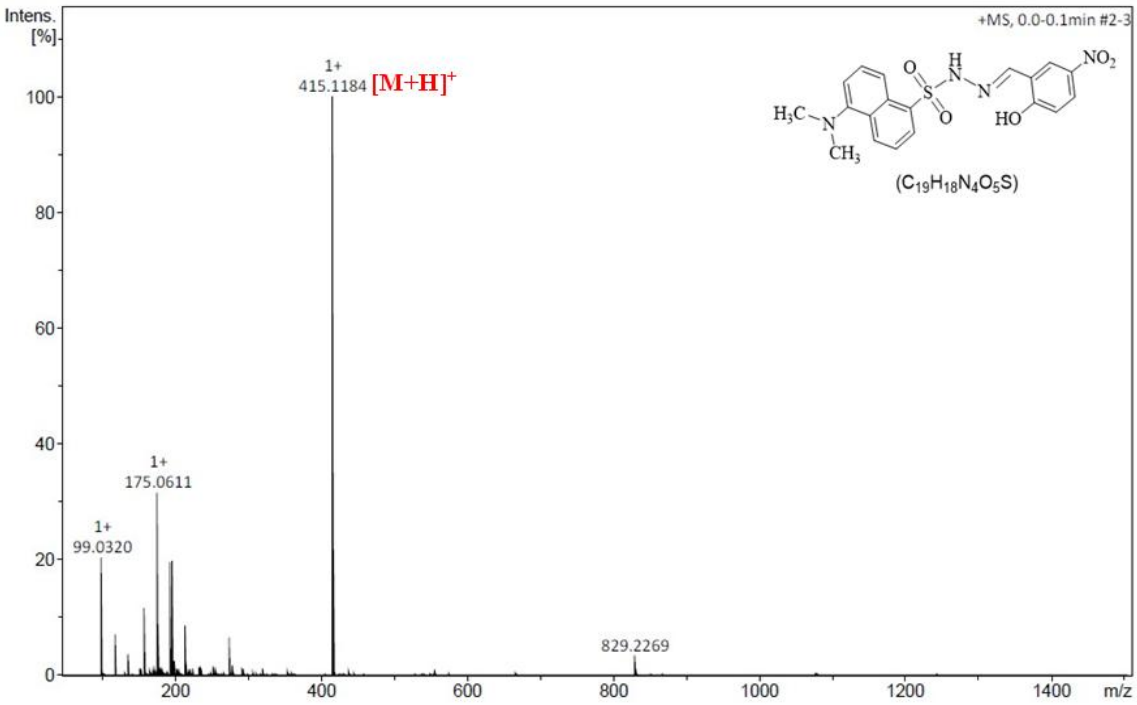

Figure S3. HRMS spectrum of compound **DHNB**.

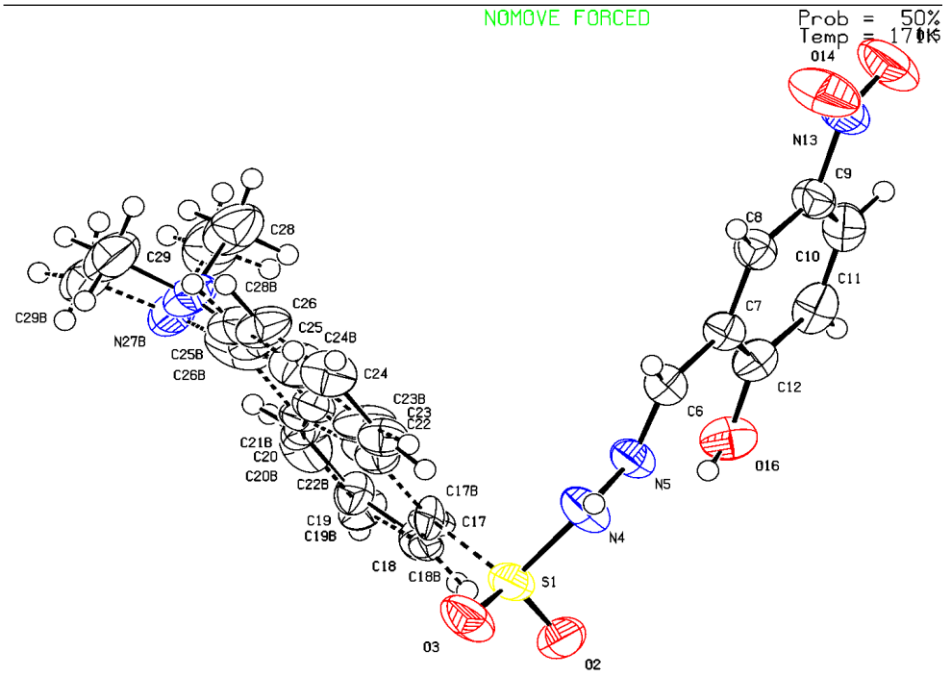

Figure S4. Asymmetric unit of **DHNB**. Displacement ellipsoids are drawn at the 50% probability level.

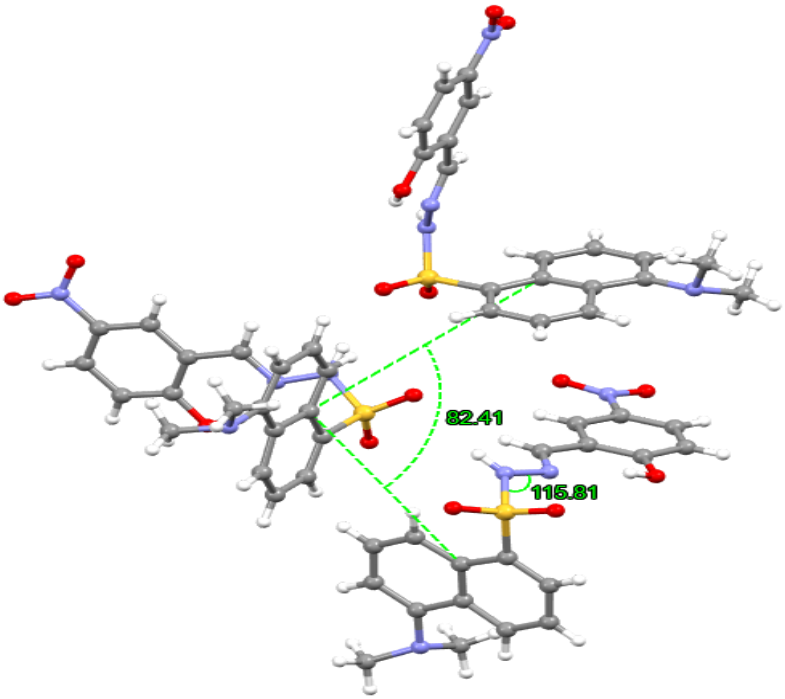

Figure S5. X-ray structure of **DHNB** showing different angles responsible for its V-shaped arrangement leading **DHNB** to exist in a slanted orientation.

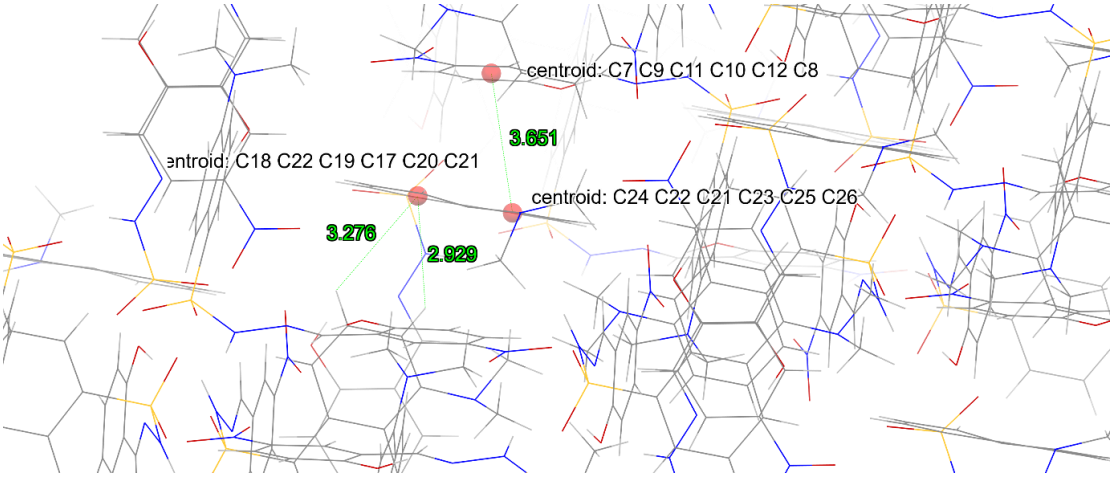

Figure S6. The packing arrangement stabilized by C–H···π interactions between naphthalene rings of neighbouring molecules, alongside π···π stacking interactions between the naphthalene moieties and the 2-hydroxy-5-nitrobenzaldehyde units.

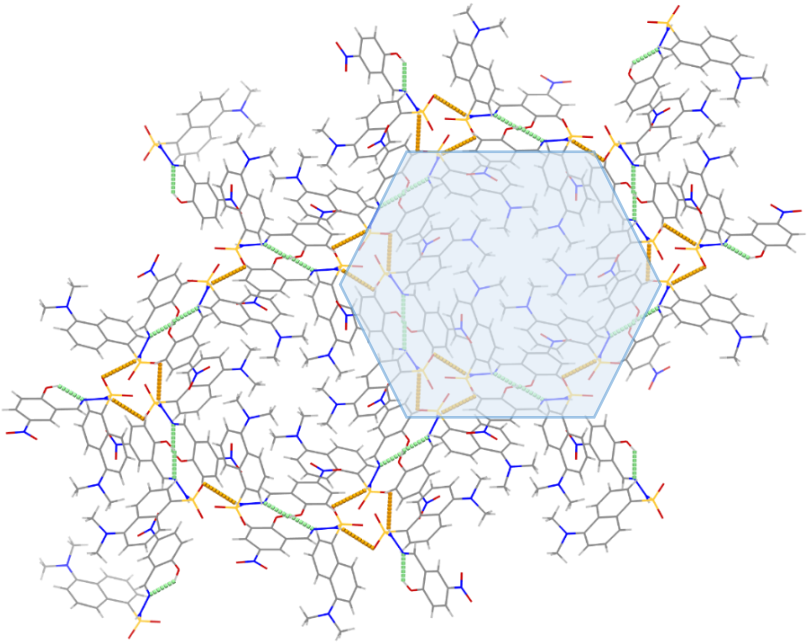

Figure S7. Packing arrangement of **DHNB** along the *c*-axis, showing intramolecular and intermolecular hydrogen bonds. The structure forms a hexagonal arrangement, with hydrophobic N-methyl groups oriented toward the inner core of the assembly.

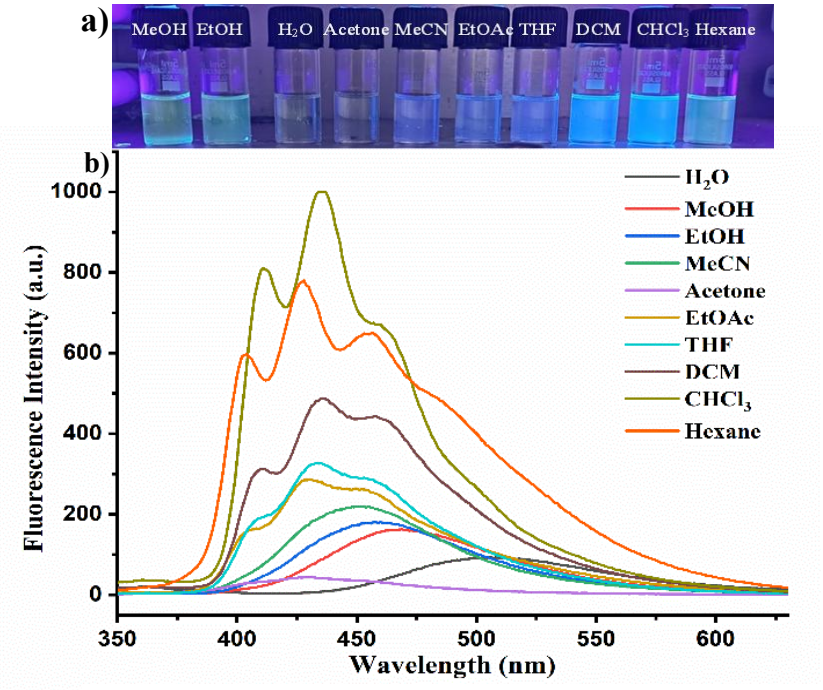

Figure S8. a) DHNB in different solvents captured under 365 nm UV illumination; **b)** Fluorescence emission spectra of **DHNB** (5.0 μM) in different solvents (λ_{ex} = 326 nm).

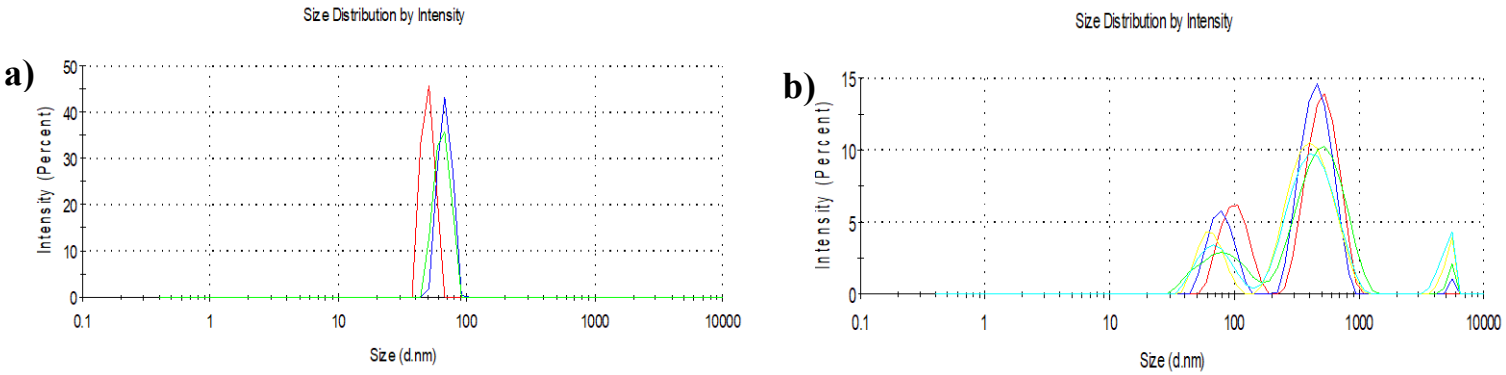

Figure S9. DLS graph of **DHNB** in **a)** 100% MeOH showing average particle size of 63 nm (PDI = 0.13); **b)** MeOH:H_2O (10:90) showing broad particle size distribution (PDI = 0.87).

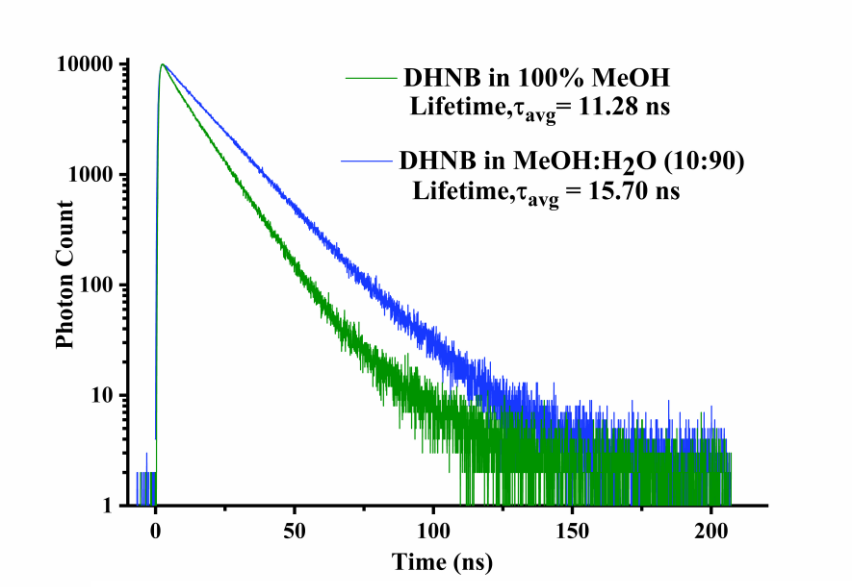

Figure S10. Fluorescence lifetime decay curve of **DHNB** in 100% MeOH *vs* in MeOH:H_2O (10:90).

Table S1. Comparative table of PPD and BWB detection performance of the present work to other fluorescent probes.

Fluorescent Sensor	**Selectivity towards BWB**	**Limit of Detection**	**Ref.**
Formyl boronate ester	Not tested	30 µM	[1]
PFPE-COOH	Not tested	89 µM	[2]
FDAC	Not tested	3.2 µM	[3]
MOF-based nanozyme	Not tested	1.0 µM	[4]
DHNB	**Differential fluorescence behaviour to PPD**	**PPD = 12.5 µM BWB = 10.2 µM**	**This work**

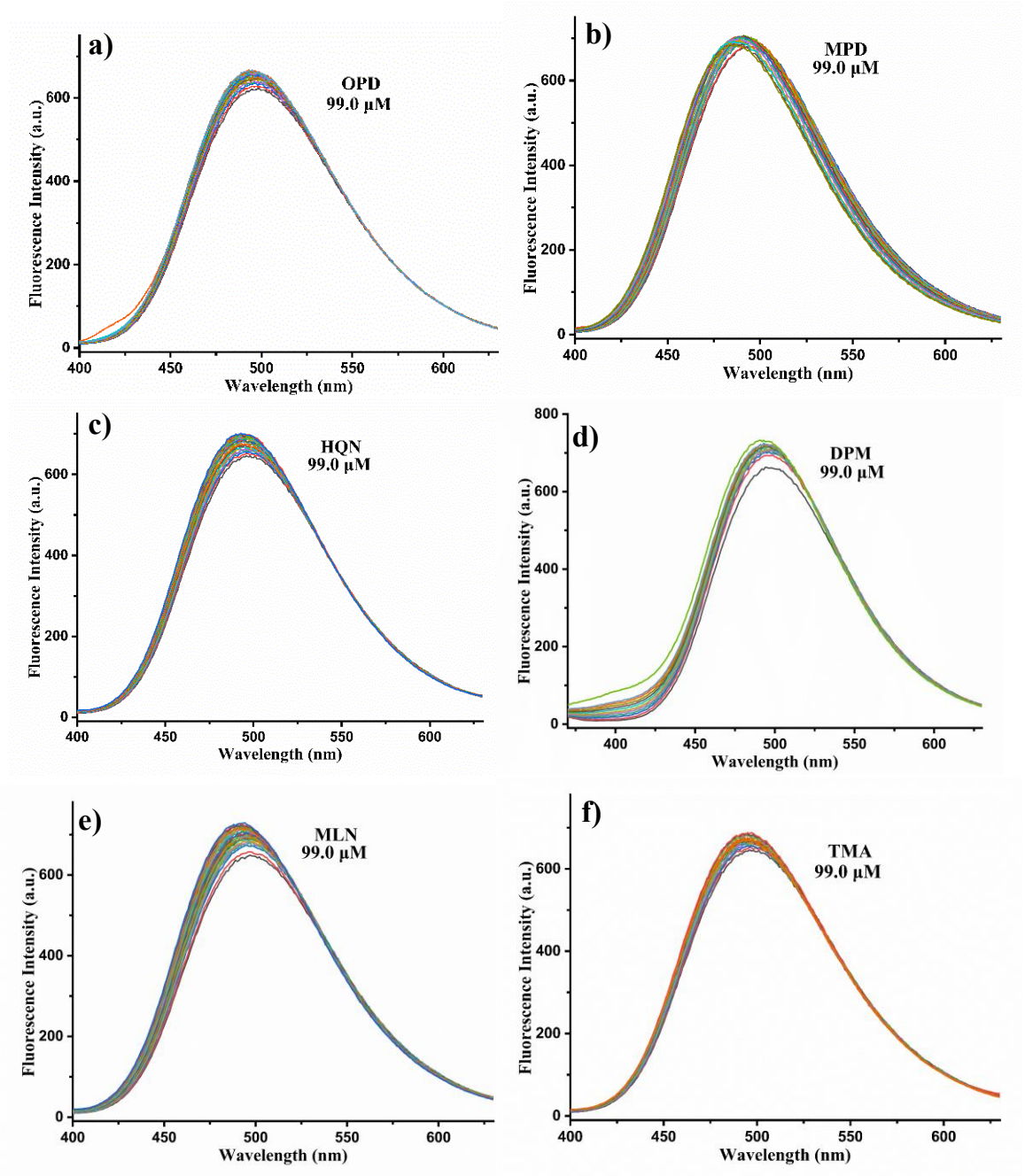

Figure S11. Fluorescence emission spectra of **DHNB** (5.0 µM) in MeOH:H_2O (10:90) upon addition of increasing concentration **a)** OPD (99.0 µM) **b)** MPD (99.0 µM) **c)** HQN (99.0 µM) **d)** DPM (99.0 µM) **e)** MLN (99.0 µM) **f)** TMA (99.0 µM) (λ_{ex} = 326 nm).

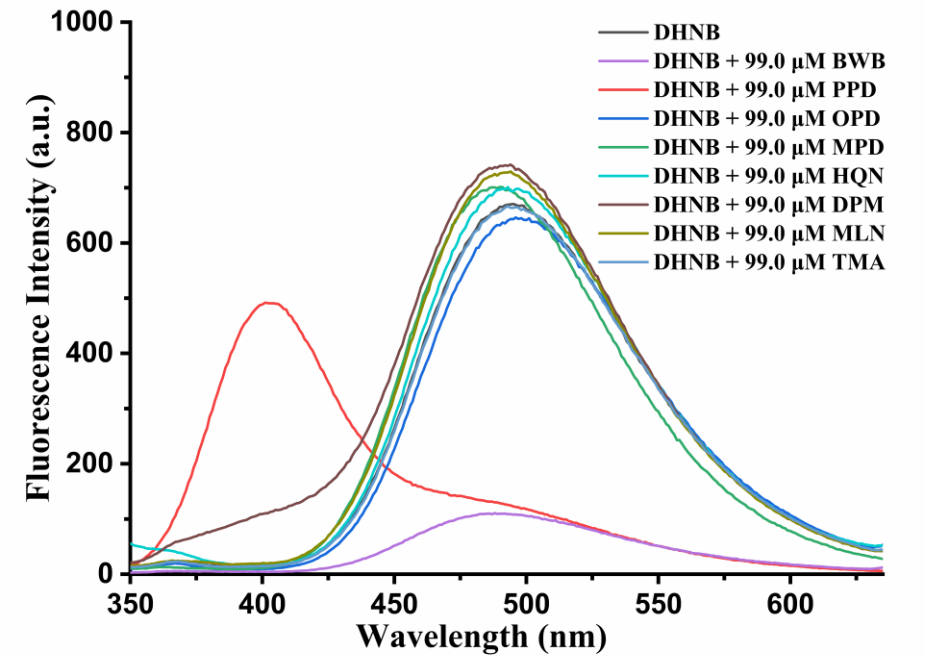

Figure S12. Changes in fluorescence emission of 5.0 µM **DHNB** in MeOH:H_2O (10:90) upon addition of 99.0 µM concentration of various analytes (λ_{ex} = 326 nm).

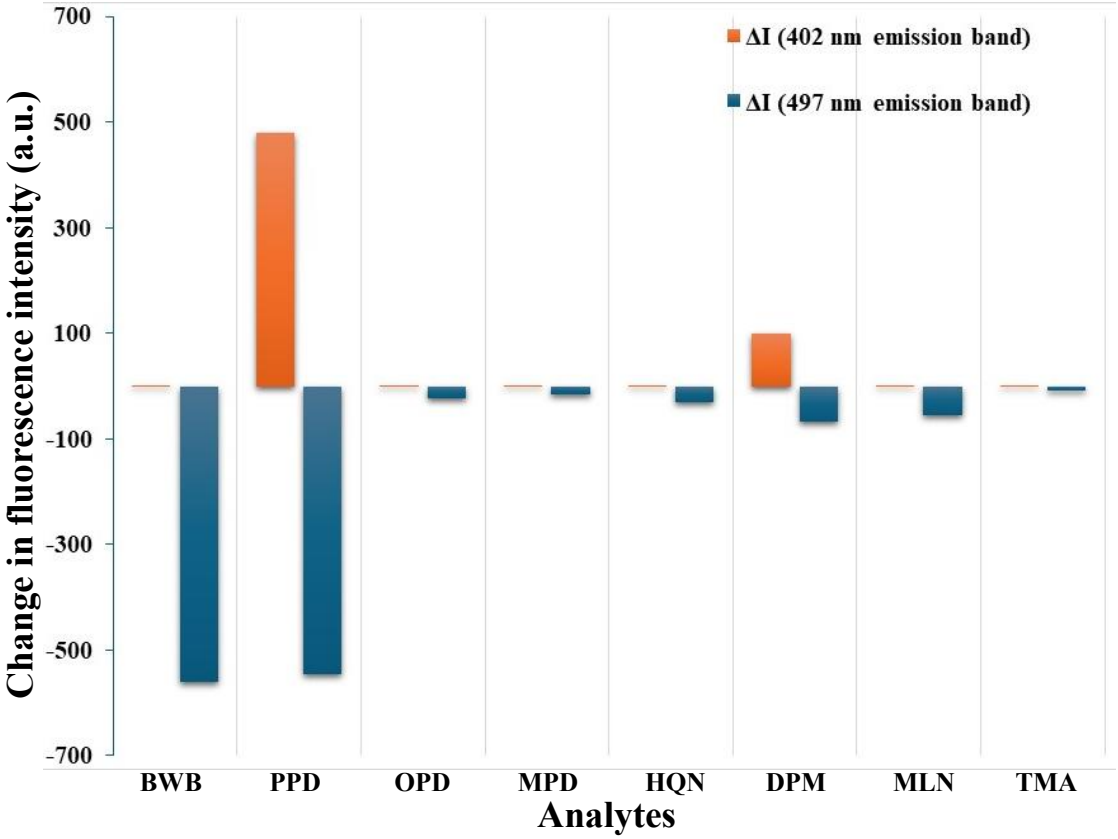

Figure S13. Bar graph showing fluorescence emission enhancement at 402 nm and fluorescence quenching at 497 nm emission bands of 5.0 µM **DHNB** in MeOH:H_2O (10:90) upon addition of 99.0 µM concentration of various analytes.

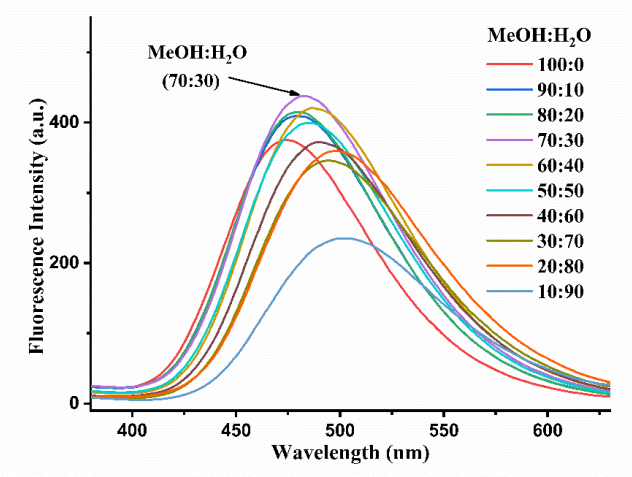

Figure S14. Fluorescence emission spectra of **DHSD** (5.0 μM) in varying % (MeOH:H_2O) fractions (λex = 340 nm).

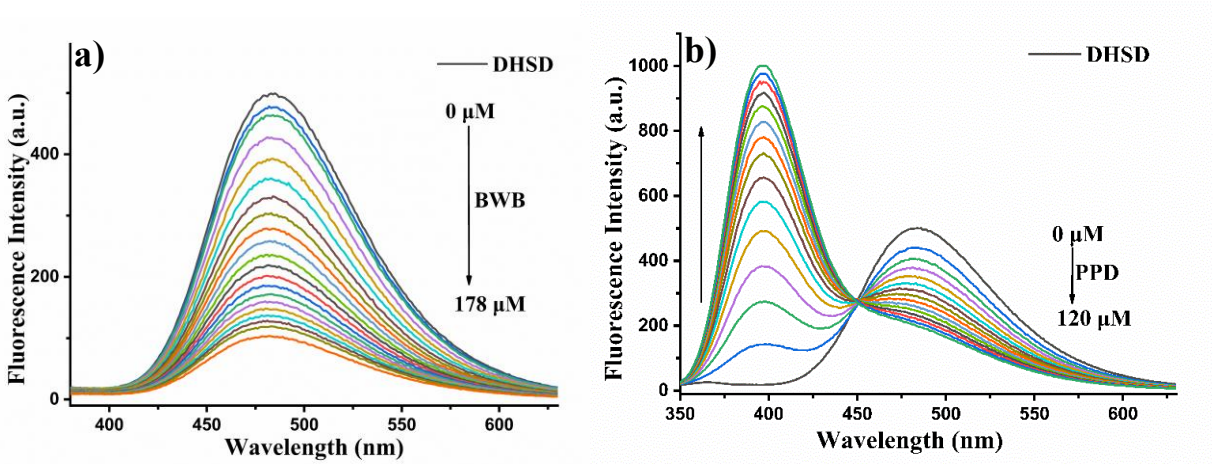

Figure S15. Fluorescence emission spectra of **DHSD** (5.0 μM) in MeOH:H_2O (70:30) upon addition of increasing concentration **a)** BWB (178.0 μM), **b)** PPD (120.0 μM) (λ_{ex} = 340 nm).

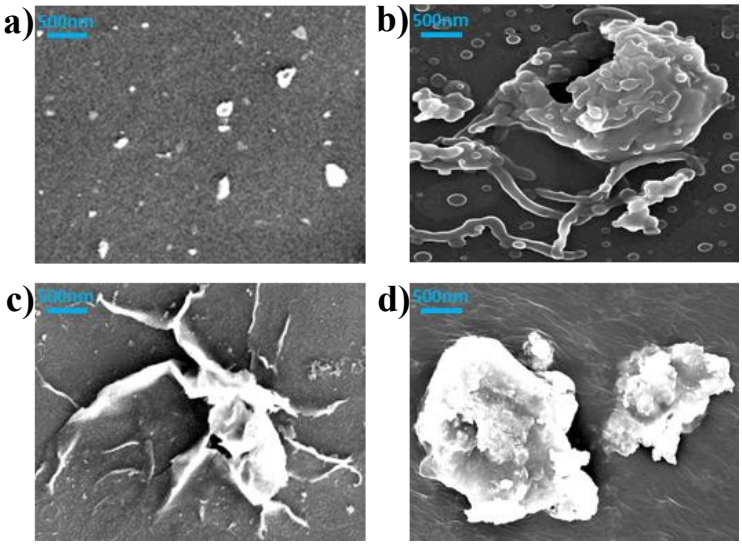

Figure S16. SEM images of **DHSD** in **a)** 100% MeOH; **b)** MeOH:H_2O (70:30); **c)** MeOH:H_2O (70:30) upon addition of PPD; **d)** MeOH:H_2O (70:30) upon addition of BWB.

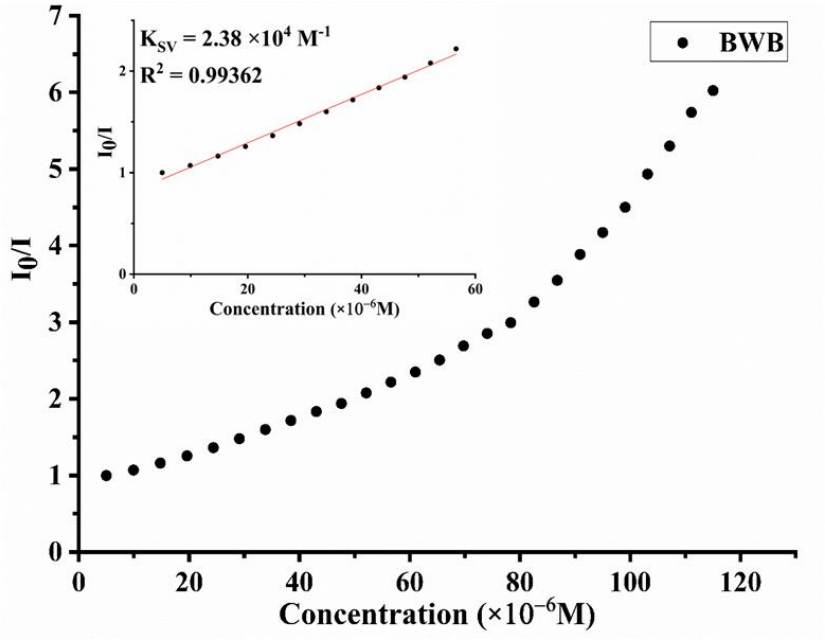

Figure S17. Stern-Volmer plot showing fluorescence response of **DHNB** towards BWB**.** Inset: Linear fit of the plot at low concentration of BWB.

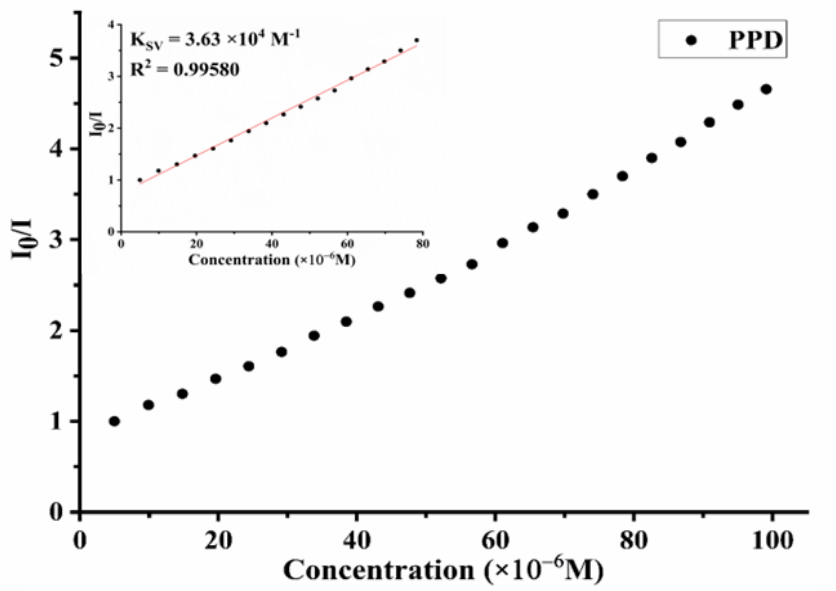

Figure S18. Stern-Volmer plot showing fluorescence response of **DHNB** towards PPD**.** Inset: Linear fit of the plot at low concentration of PPD.

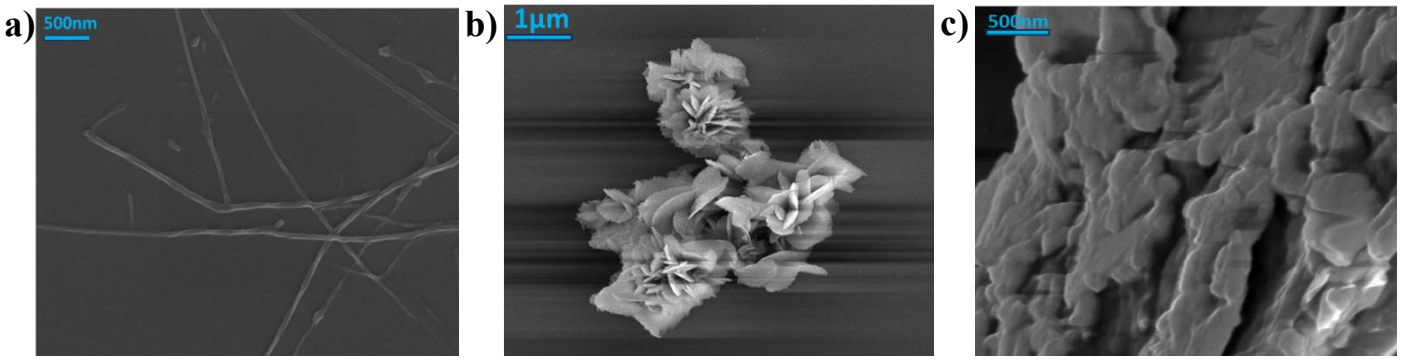

Figure S19. SEM image of **a) DHNB** in MeOH:H_2O (10:90); **b) & c) DHNB** in MeOH:H_2O (10:90) upon BWB addition.

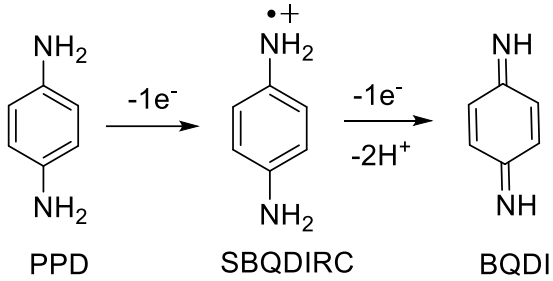

Figure S20. BQDI formation from PPD *via* two one-electron steps through intermediate SBQDIRC.

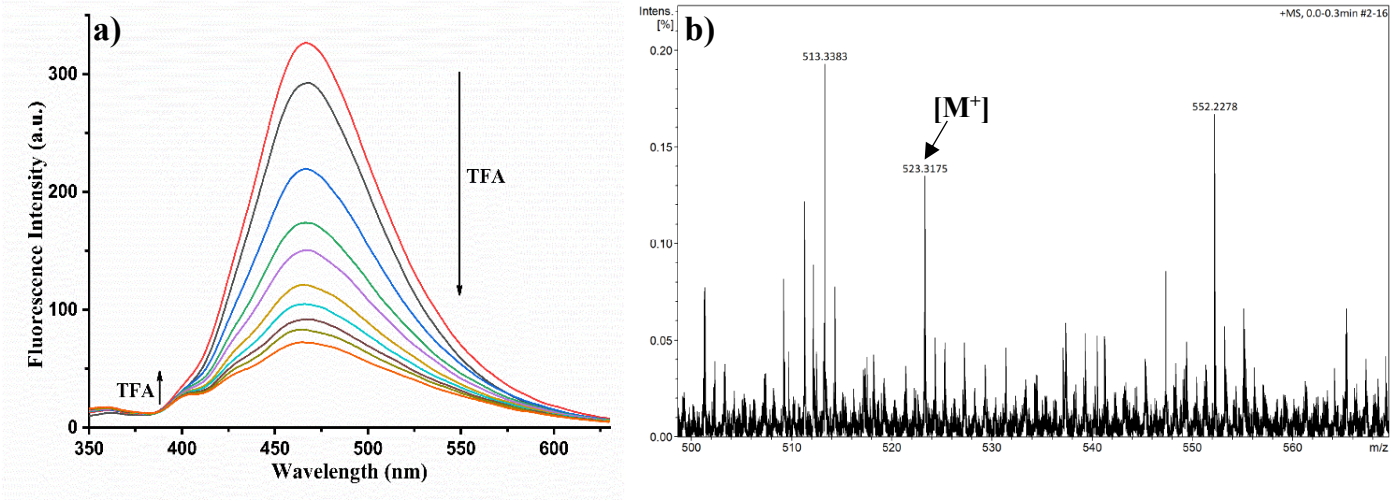

Figure S21. a) DHNB in 100% MeOH titrated against trifluoroacetic acid (TFA); **b)** HRMS of **DHNB** +PPD solution.

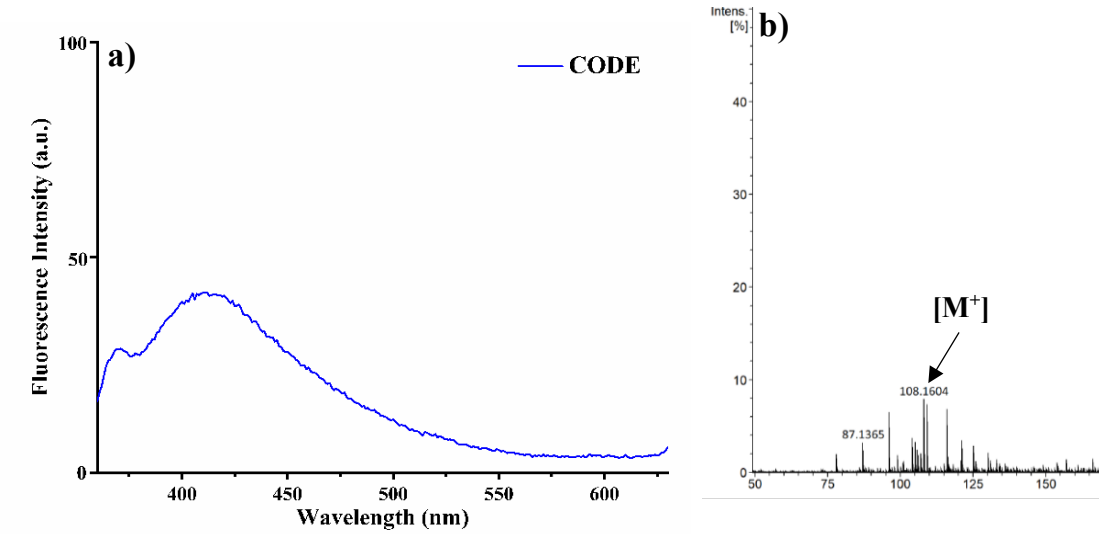

Figure S22. a) Fluorescence emission spectra of CODE solution (λ_{em} = 415 nm) corresponding to PPD in H_2O emission. **b)** HRMS of CODE solution showing peak at $[M^+]$ = 108.

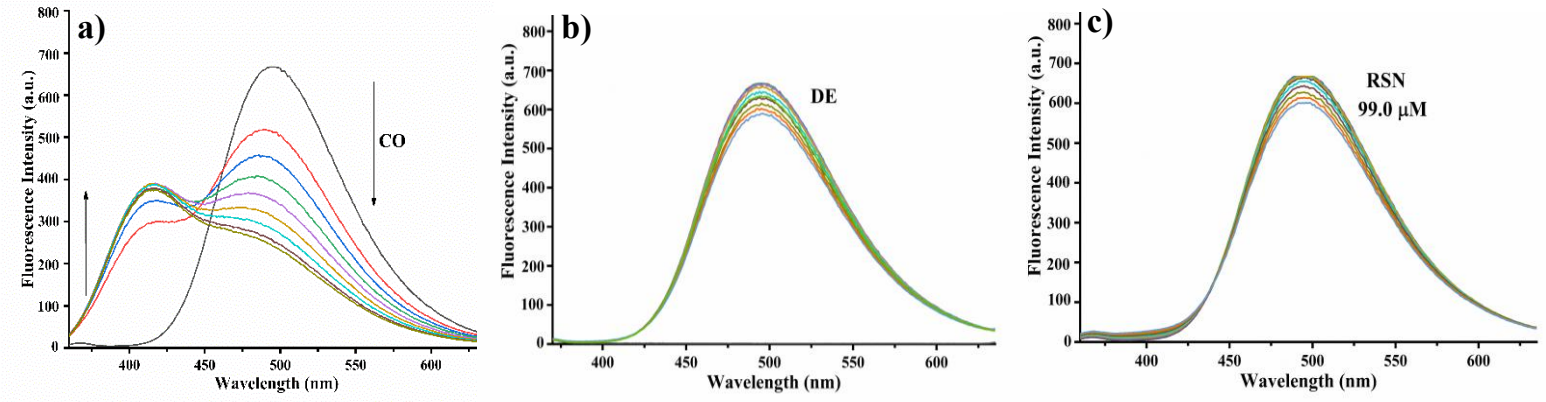

Figure S23. Fluorescence emission spectra of **DHNB** (5.0 µM) in MeOH:H_2O (10:90) upon addition of increasing extracted supernatant volumes of **a)** CO (colorant); **b)** DE (developer); **c)** RSN (resorcinol) (λ_{ex} = 326 nm).

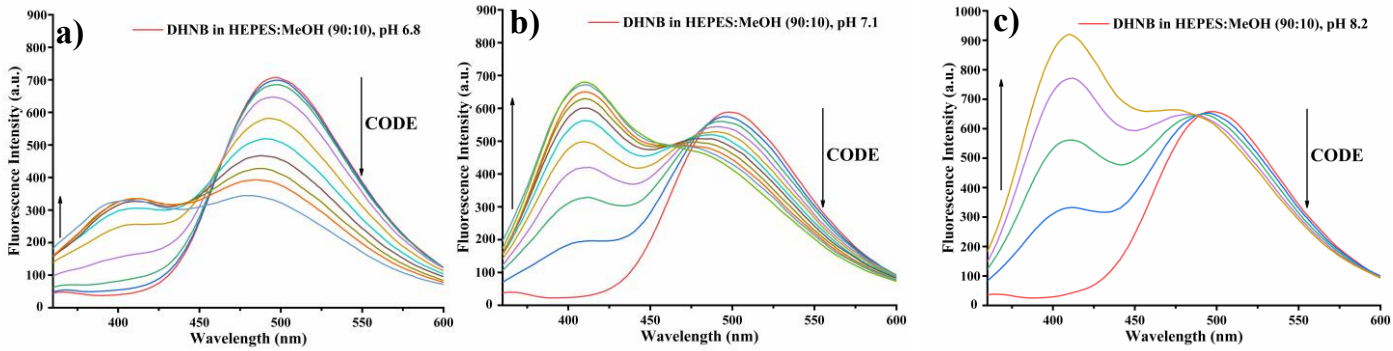

Figure S24. Fluorescence spectra of **DHNB** (5.0 µM) in HEPES:MeOH (90:10, v/v) adjusted to pH **a)** 6.8; **b)** 7.1; **c)** 8.2, upon addition of increasing volume of CODE solution (λ_{ex} = 326 nm).

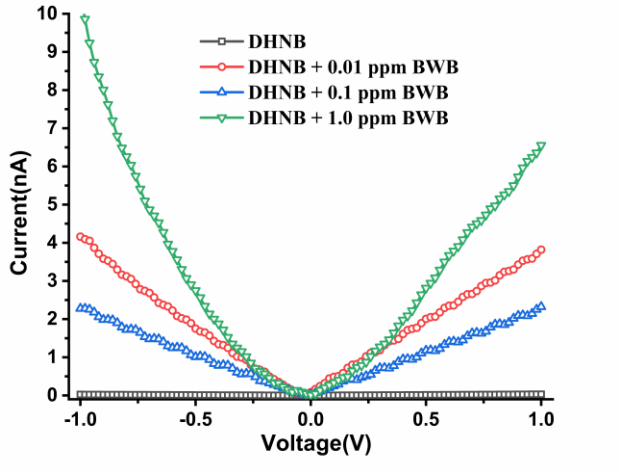

Figure S25. I-V plot of **DHNB** upon addition of increasing concentration of BWB (1.0 ppm) (Voltage range: -1.0 V to +1.0 V).

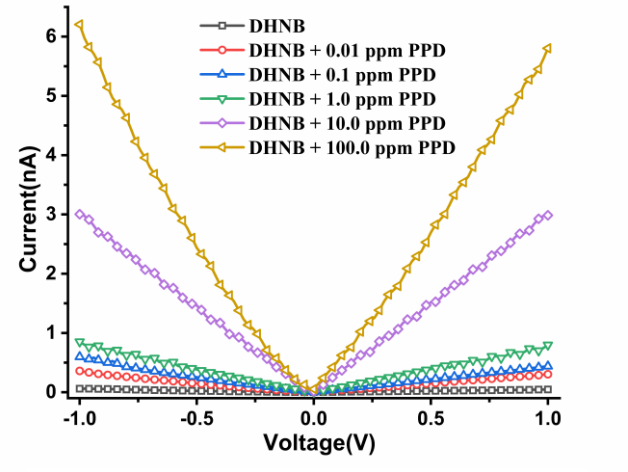

Figure S26. I-V plot of **DHNB** upon addition of increasing concentration of PPD (100.0 ppm) (Voltage range: -1.0 V to +1.0 V).

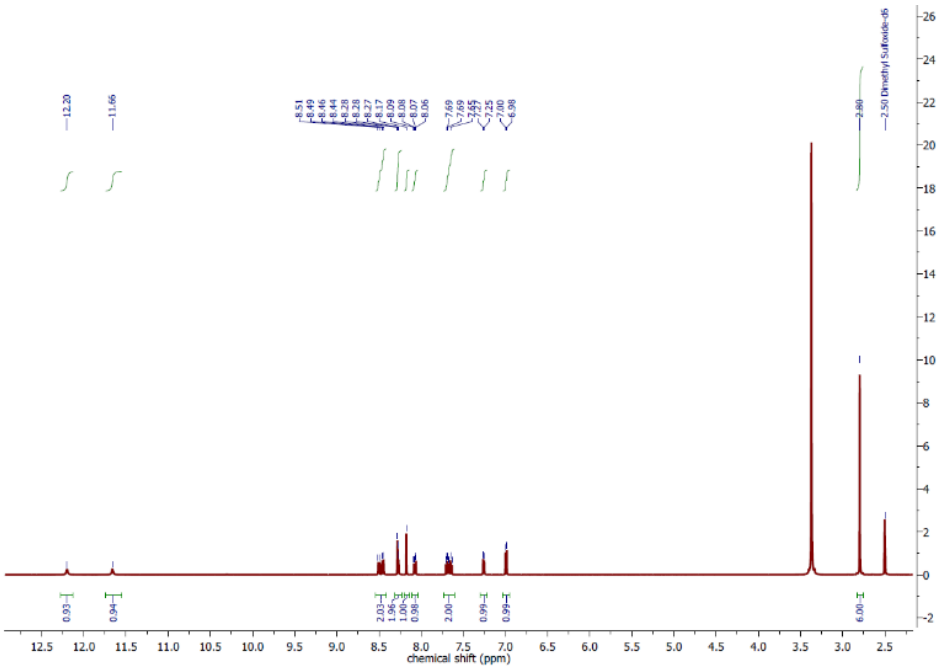

Figure S27. ^{1}H NMR spectrum of compound **DHNB** in DMSO-d_6 obtained after storage of ≈5 months.

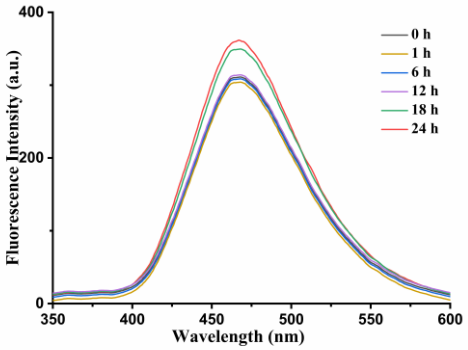

Figure S28. Fluorescence emission spectra of **DHNB** (5.0 μM) in MeOH kept under constant 365 nm UV illumination, recorded at different time intervals (λ_{ex} = 326 nm).

Table S2 Crystal data and structure refinement for DHNB:	
Identification code	DHNB
Empirical formula	$C_{19}H_{18}N_4O_5S$
Formula weight	414.43
Temperature (K)	171(2)
Wavelength (Å)	0.71073
Crystal system	Trigonal
Space group	R-3
a(Å)	30.769(14)
b(Å)	30.769(14)
c(Å)	11.003(8)
α/°	90
β/°	90
γ/°	120
Volume($Å^3$)	9021(10)
Z	18
$\rho_{calc}g/cm^3$	1.373
μ/mm^{-1}	0.200
F(000)	3888
Crystal size (mm^3)	0.11x0.10x0.08
2Θ range for data collection/°	2.293 to 25.243
Reflections collected	26085
Independent reflections	3612 [R(int) = 0.0807]
Completeness to q = 25.242° (%)	99.6
Absorption correction	Semi-empirical from equivalents
Max. and min. transmission	0.6222 and 0.4593
Refinement method	Full-matrix least-squares on F^2
Data/restraints/parameters	3612/145/384
Goodness-of-fit on F^2	1.111
Final R indices [I>2s(I)]	R_1 = 0.0680, wR_2 = 0.1676
R indices [all data]	R_1 = 0.0811, wR_2 = 0.1844
Dr (max, min) e.$Å^{-3}$	0.475, -0.377

Table S3 Selected Hydrogen Bonding interactions in DHNB [Å and °]						
D	**H**	**A**	**d(D–H)**	**d(H···A)**	**d(D···A)**	**<(DHA)**
O16	H16	N5	0.84	1.96	2.645(5)	138
N4	H4	O2	0.88	2.68	3.439(6)	145

References:

1 K. Ngamdee, S. Martwiset, T. Tuntulani, W. Ngeontae, *Sens. Actuators, B*, **2012**, *173*, 682–691.

2 Y. J. Zhao, K. Miao, Z. Zhu, L. J. Fan, *ACS Sens.*, **2017**, *2*, 842–847.

3 X. Wang, Y. Bai, Q. He, J. Li, S. Wang, W. Guo, X. Sun, *Int. J. Biol. Macromol.*, **2024**, *254*, 127783.

4 Y. Xia, K. Sun, Y. N. Zuo, S. Zhu and X. E. Zhao, *Chin. Chem. Lett.*, **2022**, *33*, 2081–2085.